ROBUST FEATURE EXTRACTION FOR HYPERSPECTRAL IMAGERY USING BOTH SPATIAL AND SPECTRAL REDUNDANCIES

Jorge E. Pinzón[1], Susan L. Ustin[2], John F. Pierce
[1] Dept. of Applied Mathematics, [2] Dept. of Land, Air, and Water Resources,
University of California Davis, CA, 95616
[3] [2]KT-Tech, Inc., 9801 Greenbelt Road, Suite 314, Lanham MD 20706

1 INTRODUCTION

As we move into the next century, a wide range of new satellites and airborne sensors will become available with a variety of interesting problems for data analysis and signal processing. In particular, hyperspectral sensors with both, a large set of spatially contiguous spectra and a large set of spectrally contiguous images will require new techniques that ideally would treat the spatial and spectral patterns in the data simultaneously. Resolving the significant spectral and spatial properties associated to ecological processes and interactions is critical to successful interpretation of remote sensing data.

In hyperspectral images is desirable to classify images within the conventional frame of reference of field and laboratory observations with methods that avoid intrinsic singular problems. In this respect, spectral mixture analysis (SMA) has become a well established procedure for analyzing imaging spectrometry data (Ustin et al., 1993; Ustin et al., 1994; Roberts et al., 1990; Sabol et al., 1990; Gamon et al., 1993). SMA is a structured and integrated framework that simultaneously addresses the mixed-pixel problem, calibration, and variations in lighting geometry and displays the results in terms of proportions of endmembers that can be related easily to standard ecological observational units (e.g., cover). The general form of the SMA equation for each band is expressed as:

$$R_b = \sum_{em=1}^{N_e} F_{em} R_{em,b} + E_b \tag{1}$$

where R_b is the radiance at band b, F_{em} is the fraction coefficient of each endmember R_{em} weighting their radiance at band b, and E_b is an error term accounting for the unmodeled radiance in band b. Endmembers are chosen to explain the spectrally distinct materials that form the convex hull of the spectral volume. This approach works best when describing a few spectral types that, in various mixtures, can account for most of the variance in an image data set. It does not mean, however, that it is possible to identify any specific material. SMA works less well when the spectral features of interest are minor components of the total variance. In fact, SMA has the disadvantage, at least for this application, of approximating linearly the natural (non-linear) complexity of materials represented by the mixture of endmembers. This produces a non-unique mixing model to identify and quantify materials that occur at the sub-pixel scale (Sabol et al., 1992). In summary, the technique is relatively insensitive to subtle absorption features, and produces significant quantification errors due to endmember variability from linear and nonlinear mixtures (e.g. from scattering, and lighting geometry) in a pixel.

Boardman (Boardman, 1994), used a geometric approach based on the convex hull of the spectra projected into the mixing space to find a solution that minimized spectral variation for some features while accentuating others. His technique is still a SMA approach that automatically derives the number of

endmembers and estimates their pure spectral composition (Boardman, 1994), but it is suboptimal in the presence of multiple mixing. More recently, Harsanyi and Chang (Harsanyi and Chang, 1994) developed a mixture technique that rejects undesired interference by performing an orthogonal subspace projection (**OSP**). This technique simultaneously reduces data volume and emphasizes the presence of a signature of interest. Bolster et al. (Bolster et al., 1996) seeking the same goals, instead use the first difference partial least squares regression (**PLS**) that is based on a singular value decomposition (**SVD**) of the whole spectrum data set. SVD reduces noise-related interference, common in a first difference analysis, and reduces the analysis into a smaller set of independent variables. Both, OSP and PLS, achieve good performance in detecting material abundances at low levels for a particular scenario by incorporating the variability of the material abundance into the more important independent variables (factors) but they are unable to extend the application to other scenarios. In order to develop a directed search methodology to locate the desired robustness (analytic) property, Smith et al. (Smith et al., 1994) proposed a revised SMA technique, that they termed Foreground/Background Analysis (**FBA**). Harsanyi's approach shares the properties of orthogonal space projection and a similar rationale with the FBA technique. In this technique, spectral measurements are divided in two groups of foreground and background spectra that comprise a selected subset of spectra which emphasizes the presence of a signature of interest. In defining both groups they do not include intermediate mixtures between foreground and background. In that way, FBA vectors should be sensitive to minor sources of foreground spectral variation and insensitive to background spectral variation. The goal of FBA is to project spectral variation along the most relevant axis of variance that maximizes the spectral differences between the foreground and background, while minimizing spectral variation within each group. Their FBA approach defines a weighting vector $w = (w_1, w_2, \ldots, w_{Nb})$, with components w_b at each channel $b = 1, \ldots, Nb$, such that all foreground spectral vectors, $R_f = (R_{f,1}, R_{f,2}, \ldots, R_{f,Nb})$, are projected to 1 while background spectral vectors, R_b, to 0. This property is defined by the FBA system of equations:

$$\sum_{b=1}^{Nb} w_{F,b} R_{F,b} + T = 1 \qquad \textit{foreground} \tag{2}$$

and

$$\sum_{b=1}^{Nb} w_{B,b} R_{B,b} + T = 0 \qquad \textit{background}$$

where T provides a translation that is typically required to optimize the FBA system. As stated FBA is in essence another linear classifier of the spectra that can be applied to identify low and high material abundances. Pinzón et al. (Pinzón et al., 1994; Pinzón et al., 1995) modified the FBA linear system to project a subset of spectra into relevant axis of continuous property variation, like chemical content.

In this paper, we present a supervised classification technique that discriminates broad categories of materials of the surface in terms of ground truth features, such as vegetation characteristics, and soil properties. The actual relationships between these two ecological units are often difficult to resolve with respect to understanding which of many potential interacting factors is significant in a particular locality. We decompose the interaction between the spatial and spectral domains associated to these units by using wavelet tools and a hierarchical foreground background analysis (HFBA). Wavelets provide spatial coherence information that should allow us to generalize the results from the spectral features extracted by HFBA.

2 METHODS

For most purposes the problem of supervised classification can be formulated as follows: given an *input space* X and a desired property in an *output space* Y, there is an unknown (functional) relationship, F, between X and Y that is represented by a subset of m samples, from which one wants to guess the

$X - Y$ relationship. In general, F takes the form of a deterministic function + noise. One is given the training set of m samples and the guess functional $\widehat{F}$, the problem is to guess, using $\widehat{F}$, what output space value, $\widehat{y}$, is the most appropriate for a given input x. The precise meaning of "appropriate" can be difficult, and is measured through loss functions. A popular choice is the quadratic error function:

$$\epsilon(X,Y) = \sum_{i=1}^{m}(\widehat{F}(x_i) - y_i)^2 \tag{3}$$

The loss function and the way it is minimized determine the method used and its ability to generalize. Under this definition the problem of supervised classification has been identified by many other names, such as inductive inference, regression, statistical inference, model inversion, etc.

2.1 HFBA

Pinzón et al. (Pinzón et al., ress; Pinzón, 1996) modified the FBA system to project a subset of spectra into the most relevant axis of variation of a desired property. In this case, the system of equations is given by

$$\sum_{b=1}^{Nb} w_b R_{i,b} + T = c_i \tag{4}$$

That is, the reflectance matrix R times the FBA weighting vector w is equal to the desired ground characteristic C. The goal of this system is to relate spectral and ground variation along the most relevant axis of spectral variance. The general form of the FBA system has the form of a generic Finite Impulse Response (**FIR**) filter equation in time domain (Smith et al., 1996):

$$y(t) = \sum_{j=1}^{n} h(k)x(t - k/f_s)$$

where f_s is the sampling frequency and $h(k)$ are the Fourier series coefficients of the frequency response of the FIR filter, $H(f)$. Therefore, solving the FBA system plays similar role as the design process of a FIR filter.

To improve the detection of minor sources of spectral variation, we can apply the process iteratively obtaining a system of equations that works at different levels of accuracy. We stop at the level of the system noise. Solving each equation in the iteration system is the so called hierarchical FBA technique (**HFBA**) which derives sequentially a series of FBA vectors, with different general discriminating features. In essence, the HFBA system is an iteratively decimation process which extracts details in each of the levels.

The power of the HFBA method becomes apparent as we begin to catalogue more precisely the performance of the SVD in energy-packing and avoidance of overfitting problems due to its stability properties. First, r, the rank or dimension of the matrix R, could be estimated by examinating the number of non-zero singular values (Golub and Van Loan, 1989). Second, the decomposition $R = U\Sigma V^*$ provide an approximation of the matrix R by a sum of rank-one matrices (Golub and Van Loan, 1989). That is,

$$R = \sum_{j=1}^{r} \sigma_j u_j v_j* \tag{5}$$

Here, r is the rank of the matrix R, and σ_j its singular values, u_j, and v_j the left and right singular column vectors respectively. This is easily shown by noticing that Σ can be written as a sum of r matrices $\Sigma = \sum j = 1^r \Sigma_j$, where each Σ_j has just one nonzero entry σ_j . Then Equation 5 follows. One can find a very large number of different representations of R as a sum of rank-one matrices. However, Equation 5 represents the best approximation of R. That means that the hyper-ellipsoid with principal axis of

length σ_j's, provides a very important property: the q-th partial sum captures as much of the detail of R as possible (Golub and Van Loan, 1989). That is, the best least squared approximation of a matrix R by matrices of lower rank q ($q < r$), is given by $R_q = \sum_{j=1}^{q} \sigma_j u_j v_j*$. Third, when solving the FBA equations at each level with spectral matrices R close to rank-deficient, it turns out that most of the standard algorithms used to solve such systems have ill conditioned stability properties. In such cases, SVD is a good stable alternative (Golub and Van Loan, 1989). Computationally, SVD is more expensive than the standard methods, but more accurate and stable. This is the principle advantage of using SVD in the solution of the FBA equations: a stable method to process hyperspectral (rank-deficient) matrices R.

2.2 Wavelets

Wavelets are mathematical functions that split data (image or signal) into different scale components that provide the best approximation at each scale. The wavelet analysis starts with a function $\psi(x)$, called mother wavelet that is well localized and oscillating. By localization, we mean $\psi(x)$ decreases rapidly to zero as x tends to infinity. Oscillating requires that ψ behaves as a wave, that is, integrals of ψ and its firsts k moments be zero.

In summary, a wavelet decomposition can be seen as an application of a pair of complementary low and high pass filters, H and G respectively. Thus, a generic wavelet transform is depicted in Figure 1.

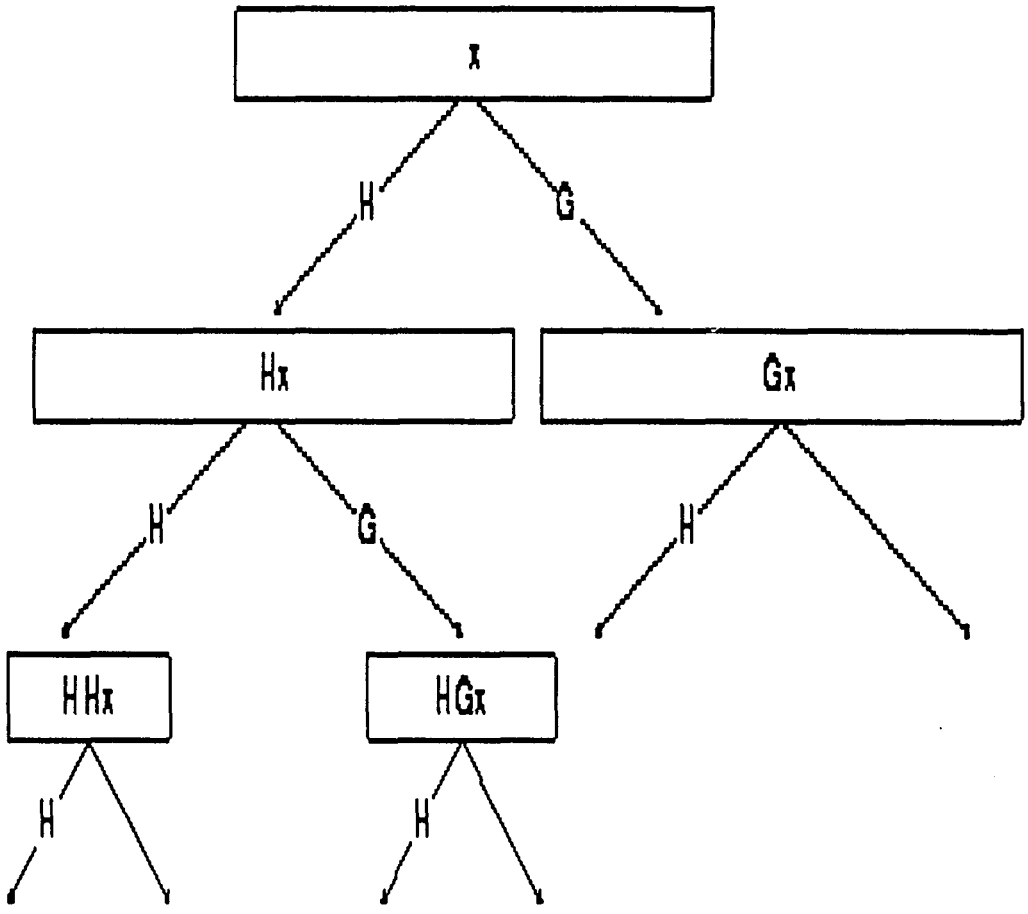

Figure 1. Discrete generic wavelet transform. From (Wickerhauser, 1994).

The properties of the wavelets are determined by the properties of the filters H and G, and by the

properties of the signal being analyzed. The construction of wavelets then begins by designing the filters that could be a basis of the space we want to transform. To lead to high compression and get coherent information we use a coiflets with 4 vanishing moments, avoiding at the same time to include noise into the estimated generalization functional, $\widehat{F}$.

3 Results

We present two applications of the HFBA: 1) retrieval of biochemical properties using laboratory spectra and chemical content of fresh leaves samples, and 2) discrimination of soil in the Santa Monica Mountains.

3.1 Retrieval of biochemical properties

For this application, we have fresh leaf samples from 3 different sites: from Santa Monica Mountains, CA, from Joint Research Center, Ispra, Italy, and from Jasper Ridge Biological Preserve at Stanford University. The samples are botanically very heterogenous, specially those in JRC. We have trained each HFBA vector with 20% of the samples from JRC and validated the results with the remaining data set. Three levels of detection were obtain, the first discriminates monocots from dicots, the second low water content from high water content and finally the actual chemical content was predicted (here we present nitrogen and water results). Monocot and dicot samples are identified by their spectral features in the visible region, where monocots are brighter due to their higher chlorophyll (a and b) content. That property is precisely the characteristic manifested in the HFBA vector, Figure 2(a). Similarly, low and high water contents are spectrally discriminated by the main water absorption features at 1400 nm and 1900 nm and their interaction in the blue visible region, Figure 2(b).

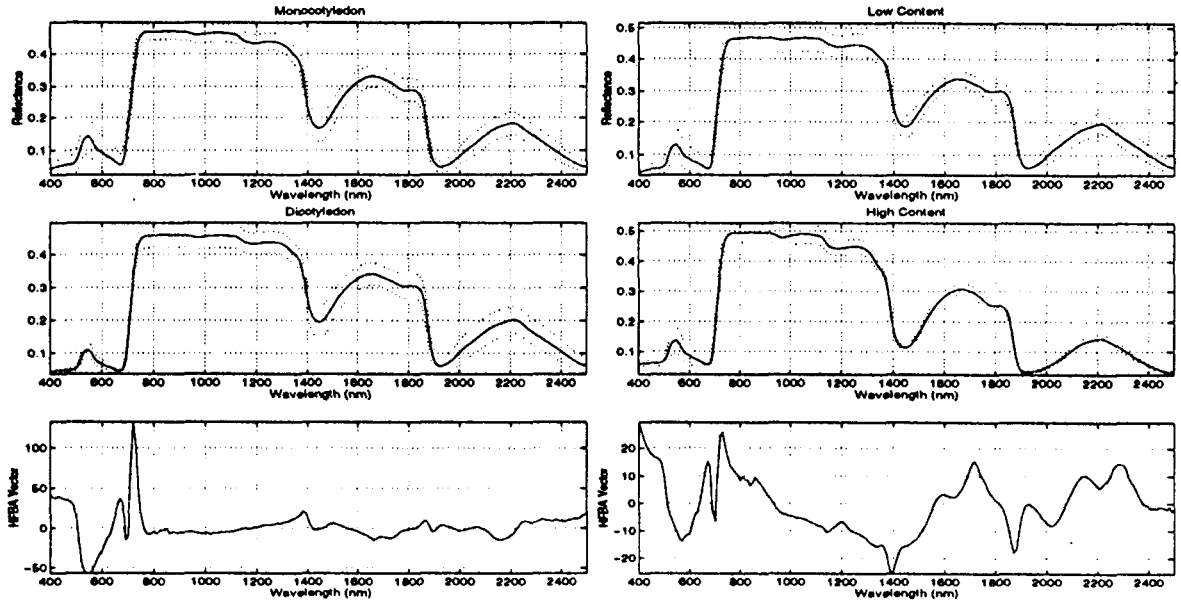

Figure 2. Classification step: (a) monocots vs dicots (b) high vs low water content

The statistics of the prediction indicates the good performance of HFBA at the laboratory level: regressions of 0.71 and 0.75 with good fit of the distribution of actual data, Figure 3.

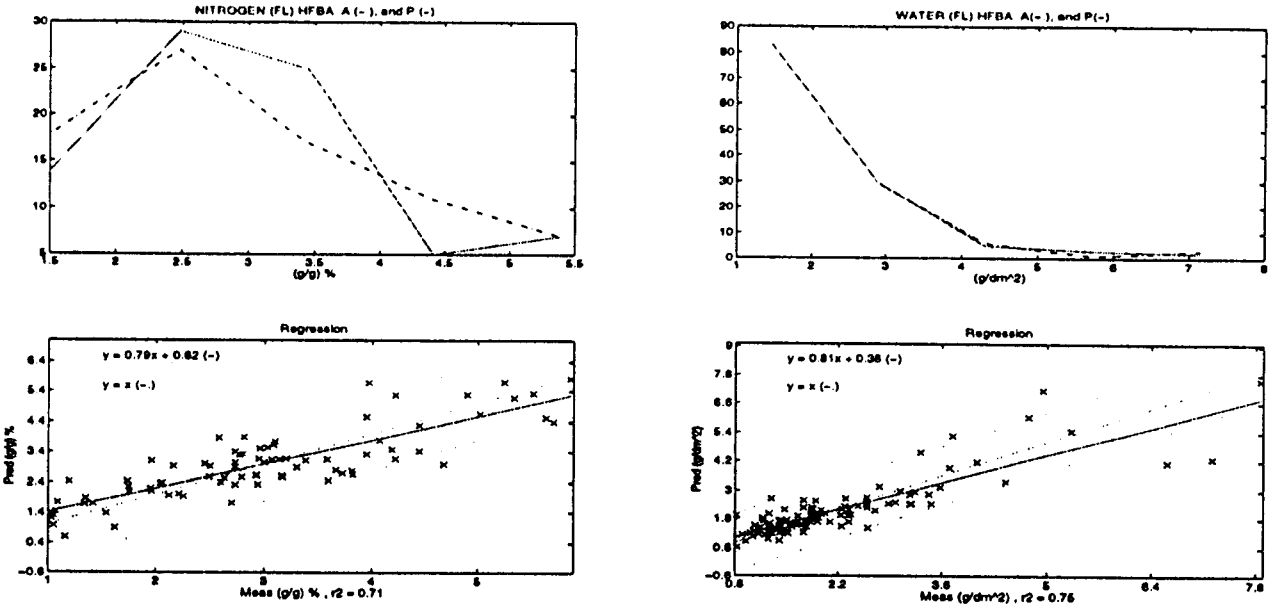

Figure 3. Retrieval of biochemical properties: (a) nitrogen concentration (b) water content.

3.2 Discrimination of Soil in the Santa Monica Mountains

We have used two levels of HFBA to discriminate soils and soil properties from two valleys in the Santa Monica Mountains (Serrano and La Jolla) using AVIRIS data. The region is highly susceptible to erosion and wildfires due to the xeric soil moisture regime typical of Mediterranean climates, as well the steep terrain. The combination of all these factors markedly increases heterogeneity in the distribution of soil properties. Large coverage and sufficient spatial resolution are required to understand soil pattern differences. AVIRIS satisfies these two requirements. The classification vector discriminates soils with high organic matter from those with low organic matter (see Figure 4). Ninety four percent of the samples were correctly classified. The other six percent show intermediate organic matter contents.

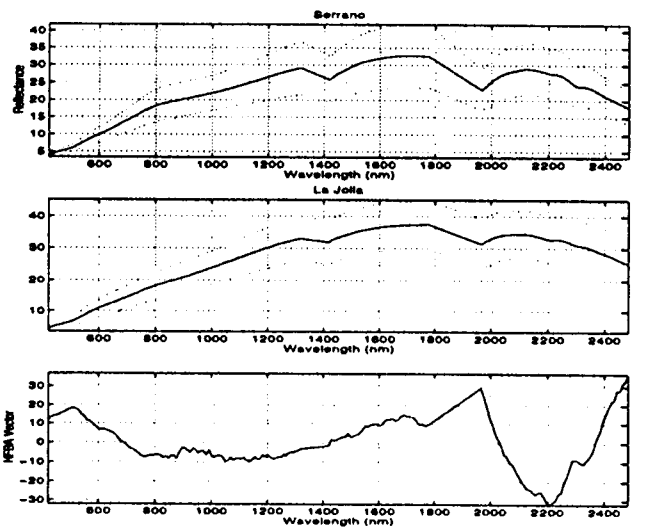

Figure 4. HFBA classification vector.

It can be observed that the two spectral areas most important for discrimination are between 1000nm and 2200nm (OH-AL and Mg-OH absorptions). The characteristic of the vector between 600 and 800 nm also could be used to detect vegetation and it will work like NDVI for this purpose. The first image in Figure 5 shows the HFBA spatial distribution. After applying coiflet wavelets (Figure 5, second row), the spatial coherence is manifested and this allows noise reduction and improves the performance of HFBA vectors. The final classification allows a better interpretation of the ecological processes involved. Image classification follows known spatial characteristics. Finally, Figure 6 shows the organic matter spatial distribution from AVIRIS data predicted by HFBA and coiflet noise reduction. High values are concentrated near ridges of the mountains as expected. It can be observed that the pixels mapped as La Jolla soils in the classification image also show high content of organic matter which agrees with our laboratory data.

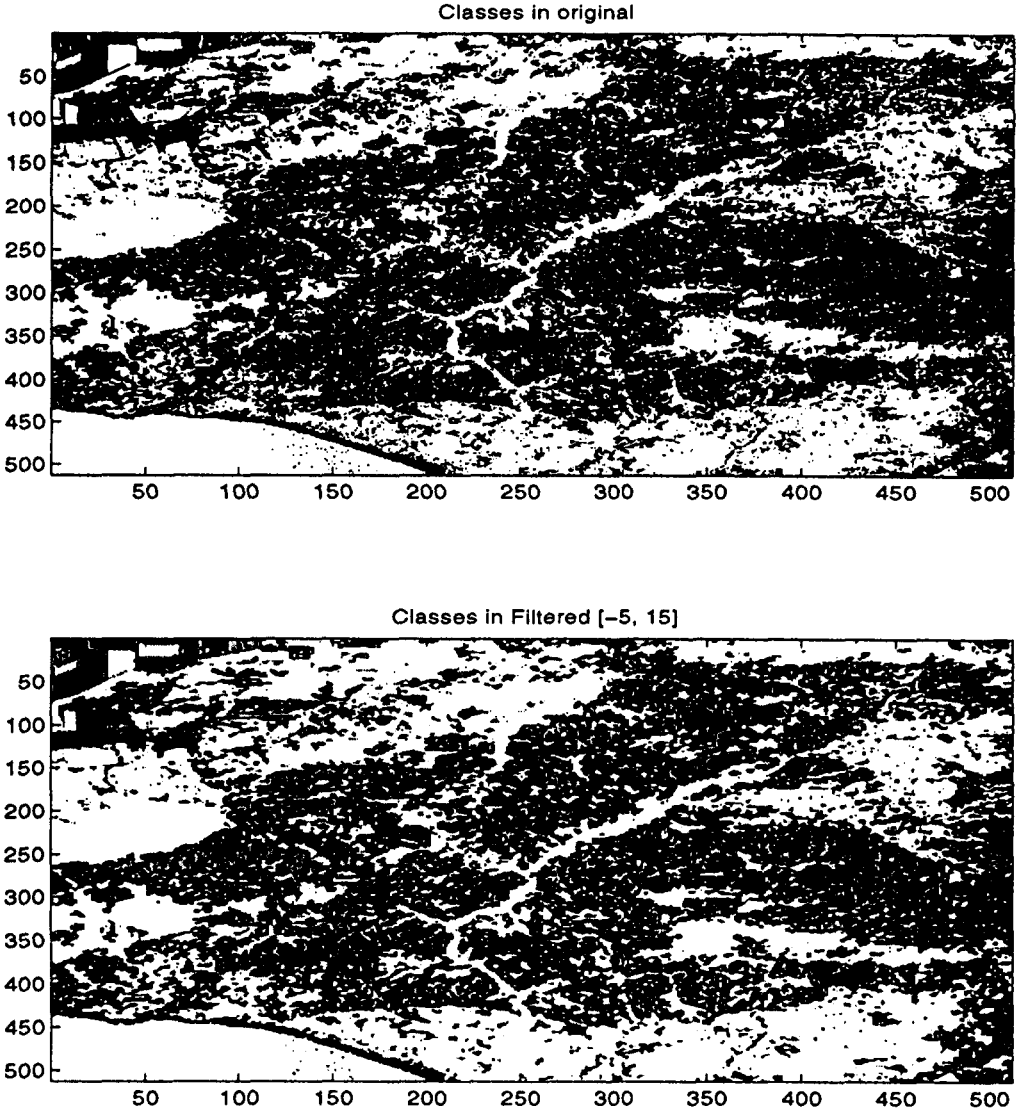

Figure 5. (a) HFBA classification and (b) spatial coherence manfested after coiflet noise reduction.

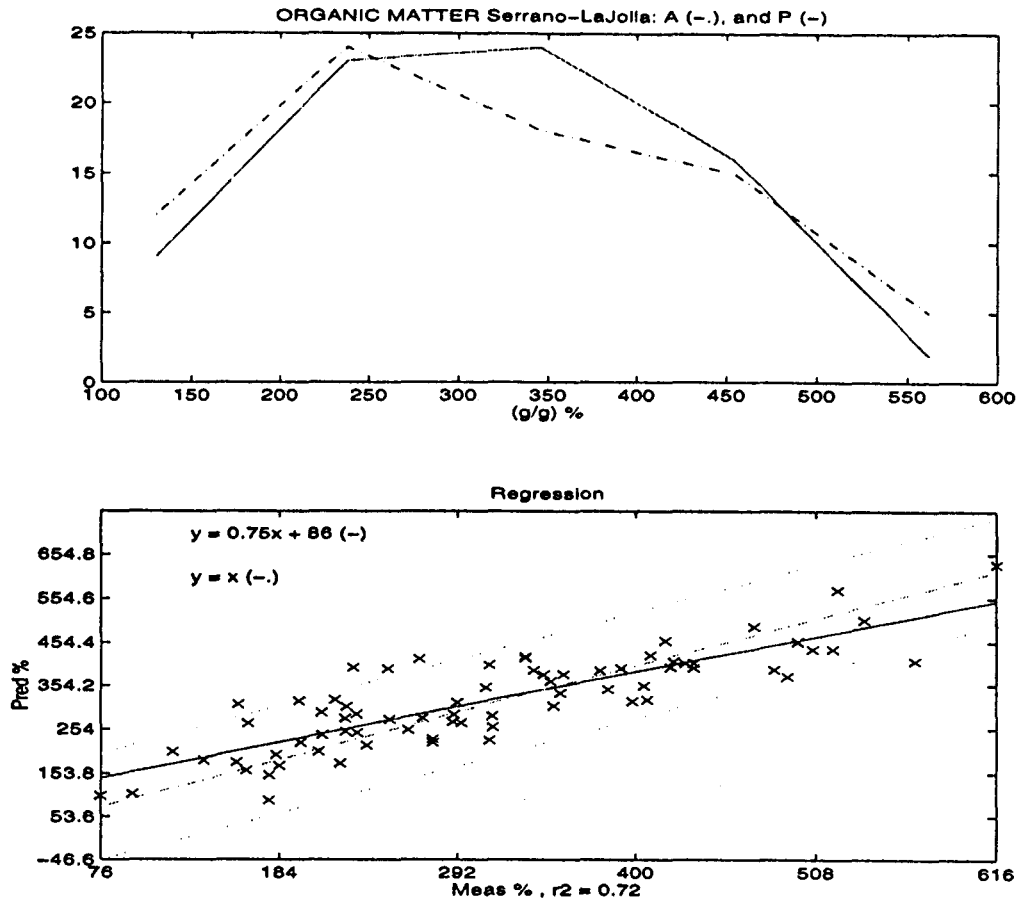

Figure 6. (a) HFBA classification and (b) spatial coherence manfested after coiflet noise reduction.

4 Conclusions

A new robust approach for the detection and classification of materials was developed and tested. The technique uses a combination of an iterative hierarchical application of a modified FBA technique and coifle noise reduction to detect functional relationships between spectra and ground truth features at different levels of accuracy.

The power of the HFBA technique is based on the attractive properties of the SVD transform in information packing and avoidance of overfitting problems by minimizing extraneous noise in the analysis. The technique was trained over laboratory data and applied to AVIRIS images. It is clear from the above experiments that the proposed approach is promising.

By the iterative hierarchical procedure we force the system to account for important non-linear dependencies directly related to spectral scaling. In that respect, one of the strong points of the proposed method is that we can group together samples with similar anatomical properties manifested spectrally. However, if the distribution of these properties is continuous, samples near the boundaries of the discriminant regions could be misclassified weakening the helpfulness of the classification step. In particular, as spatial variation of vegetation is high, the selection of a training set that explains the mixing presented at different spatial scales is critical. This process seems to be a key factor for understanding the good performance of HFBA dealing with sub-pixel scaling issues in this application, although HFBA was not properly equipped to deal directly with these spatial issues. There are more appropriate image analysis methodologies concerning spatial scaling problems such as wavelet transforms. The wavelet decomposition gives a better representation of spatial distribution (at different scales) of the data, and especially a better

description of the properties of samples near to discriminant boundaries. Clearly, these points have to be further investigated to identify the relationship between spatial-spectral scales.

As a conclusion, we consider that a combination of HFBA and wavelets or other spatial scaling transforms has significant potential and certainly deserves further investigation. There are many aspects for the discrimination among materials that still need investigation. The aspects we have in mind are aptly illustrated by Yves Meyer in his book *Wavelets: algorithms and applications* (Meyer, 1993): "It is notable that Mandelbrot used the word *describe* and not *explain* or *interpret*. We are going to follow him in this, ostensibly, very modest approach. This is our answer to the problem about the objectives of the choices: *Wavelets, whether they are of the time-scale or time-frequency type, will not help us to explain scientific facts, but they will serve to describe the reality around us, whether or not it is scientific.* Our task is to optimize the description. This means that we must make the best use of the resources allocated to us to obtain the most precise possible description."

References

Boardman, J. W.: 1994, in *IGARSS 94: Procedings International Geosciences Remote Sensing Symposium*, Vol. 4, pp 2369–2371

Bolster, K. L., Martin, M. E., and Aber, J. D.: 1996, *Can. J. For. Res.* **26**, 590

Gamon, J. A., Field, C. B., Roberts, D. A., Ustin, S. L., and Valentini, R.: 1993, *Remote Sensing of Environment* **44(2)**, 239

Golub, G. H. and Van Loan, C. F.: 1989, *Matrix Computations*, John Hopkins University Press, Baltimore, Maryland

Harsanyi, J. C. and Chang, C. I.: 1994, *IEEE Transactions on Geoscience and Remote Sensing* **32(4)**, 779

Meyer, Y.: 1993, *Wavelets: Algorithms and Applications*, SIAM press, Philadelphia

Pinzón, J. E.: 1996, *Master's thesis*, University of California, Davis, Master degree

Pinzón, J. E., Ustin, S. L., Castañeda, C. M., and Smith, M. O.: In press, *Investigation of Leaf Biochemestry by hierarchical Foreground/Background Analysis*, IEEE Transactions on Geoscience and Remote Sensing

Pinzón, J. E., Ustin, S. L., Hart, Q. L., Jacquemoud, S., and Smith, M. O.: Jan 23-27, 1995, in R. O. Green (ed.), *Proc. 5th. annual JPL Airborne Earth Science Workshop: AVIRIS Workshop*

Pinzón, J. E., Ustin, S. L., Hart, Q. L., Jacquemoud, S., and Smith, M. O.: Reno, Nevada, Nov 9-10, 1994, in *Spectral Analysis Workshop: The Use of Vegetation as an Indicator of Environmental Contamination*

Roberts, D. A., Adams, J. B., and Smith, M. O.: 1990, *Remote Sensing of Environment* **34**, 1

Sabol, D. E., Adams, J. B., and Smith, M. O.: 1990, in *Proceedings of the IEEE International Geoscience Remote Sensing Symposium 1990*, Vol. 2, pp 967–970

Sabol, D. E., Adams, J. B., and Smith, M. O.: 1992, *Journal of Geophysical Research* **97(E2)**, 2659

Smith, M. O., Roberts, D. A., Hill, J., Mehl, W., Hosgood, B., Venderbout, J., Schmuck, G., Koechler, C., and Adams, J.: 1994, in *IGARSS 94: Procedings International Geosciences Remote Sensing Symposium*, Vol. 4, pp 2372–2374

Smith, M. O., Weeks, R., and Gillespie, A.: 24-27 June, 1996, in *ERIM 96: Second International Airborne Remote Sensing Conference and Exhibition, San Francisco*, Vol. 1

Ustin, S. L., Hart, Q. J., Scheer, G., and Duan, L.: 1994, in *IGARSS 94: Procedings International Geosciences Remote Sensing Symposium*, Vol. 2, pp 1211–1212

Ustin, S. L., Smith, M. O., and Adams, J. B.: 1993, in J. R. Ehleringer and C. B. Field (eds.), *Scaling Physiological Processes: Leaf to Globe*, pp 339–357, Academic Press, San Diego

Wickerhauser, M. V.: 1994, *Adapted wavelet analysis from theory to software*, A K Peters, Ltd., Wellesley, MA

MAPPING THE DISTRIBUTION OF WILDFIRE FUELS USING AVIRIS IN THE SANTA MONICA MOUNTAINS

Dar Roberts[1], M. Gardner[1], J. Regelbrugge[2], D. Pedreros[1] and S. Ustin[3]

1. Department of Geography, EH3611, University of California, Santa Barbara, CA 93106
2. USDA Forest Service, Forest Fire Laboratory, 4955 Canyon Crest Dr., Riverside, CA 92507
3. Department. of Land, Air, and Water Resources, University of California, Davis, CA, 95616,

1 Introduction

Catastrophic wildfires, such as the 1990 Painted Cave Fire in Santa Barbara or Oakland fire of 1991, attest to the destructive potential of fire in the wildland/urban interface. For example, during the Painted Cave Fire, 673 structures were consumed over a period of only six hours at an estimated cost of 250 million dollars (Gomes et al., 1993). One of the primary sources of fuels is chaparral, which consists of plant species that are adapted to frequent fires and may actually promote its ignition and spread of through volatile organic compounds in foliage (Philpot, 1977). As one of the most widely distributed plant communities in Southern California (Weislander and Gleason, 1954), and one of the most common vegetation types along the wildland urban interface, chaparral represents one of the greatest sources of wildfire hazard in the region.

An ongoing NASA funded research project was initiated in 1994 to study the potential of AVIRIS for mapping wildfire fuel properties in Southern California chaparral. The project was initiated in the Santa Monica Mountains, an east-west trending range in western Los Angeles County that has experienced extremely high fire frequencies over the past 70 years (Office of Emergency Services, 1995). The Santa Monica Mountains were selected because they exemplify many of the problems facing the southwest, forming a complex mosaic of land ownership intermixed with a diversity of chaparral age classes and fuel loads. Furthermore, the area has a wide diversity of chaparral community types and a rich background in supporting geographic information including fire history, soils and topography. Recent fires in the Santa Monica Mountains, including several in 1993 and the Calabasas fire of 1996 attest to the active fire regime present in the area. The long term objectives of this project are to improve existing maps of wildland fuel properties in the area, link AVIRIS derived products to fuel models under development for the region, then predict fire hazard through models that simulate fire spread. In this paper, we describe the AVIRIS derived products we are developing to map wildland fuels.

2 Background

A number of studies have focused on fire hazard assessment (Cosentino et al., 1981; Burgan and Shasby, 1984; Yool et al., 1985; Chuvieco and Congalton, 1989 and Stow et al., 1993; Clarke et al., 1994). In general, remote sensing has been used to classify vegetation into fuel classes then combined through a GIS with collateral information such as slope, aspect, elevation and fire history to assess hazard (Cosentino et al., 1981; Burgan and Shasby, 1984; Yool et al., 1985; Chuvieco and Congalton, 1989 and Stow et al., 1993). For example, Chuvieco and Congalton (1989) used Landsat Thematic Mapper data to classify vegetation by fuel class then used elevation, slope, aspect and proximity to roads to generate a fire hazards index. Burgan and Shasby (1984) merged Landsat MSS, aerial photography and digital elevation data to map seven fuel classes near Missoula Montana. Fuel classes were assigned to a National Fire Danger Rating (NFDR) fuel model to calculate the Energy Release Component (ERC) (heat energy/unit area) for each image element, which was then used as a measure of hazard. Changes in fuel moisture were modeled from digital topography (e.g. insolation) and weather data to predict changes in moisture content. Cohen (1991) used laboratory reflectance data of several chaparral dominants to monitor spectral changes in foliage through a growth season. He evaluated the tasseled cap as a means of monitoring seasonal drying in vegetation as changes in greenness, brightness and wetness. Stow et al., (1993) extended the use of the tasseled cap to analyze a pair of TM scenes from the beginning and end of the 1986-1987 growing season in Southern California. Differences were stratified by vegetation community type, stand age (fire history),

and slope and aspect. They found that end of season changes in greenness for mixed chaparral varied with stand age and matched field measures of total and live standing biomass, although seasonal changes in illumination were the most dominant differences.

Imaging spectrometry, through improved characterization of the chemistry and physical properties of natural surfaces and atmospheres has the potential of significantly improving our ability to map fuels and predict fire hazard. Important fuels properties and associated remotely sensed measures are summarized in Table 1. Important AVIRIS capabilities include: 1) the ability to retrieve apparent surface reflectance in a spatially variable atmosphere, providing temporally robust measures of surface properties; 2) canopy liquid water retrievals, providing direct estimates of moisture content and; 3) improved classification of vegetation. When combined with spectral mixture models to estimate the areal proportions of live and dead crown components, these tools provide a new, unique approach to fire hazard assessment. The importance of collateral information (e.g. fire history, digital topography) for fire hazard assessment is clear: canopy depth, stand age and surface winds are all parameters of critical importance to fire modeling, yet cannot be derived from remote sensing. For this reason, GIS is a significant component of our research effort. Important GIS layers are also described in Table 1.

Table 1. Important fuel properties

Fuel Property	Remotely Sensed Measure
Total Fuel Load (kg/ha)	
Live fuels (Green leaves, live stems)	NDVI, Green Vegetation Fraction* , Liquid Water
Dead fuels (litter, stems, twigs)	Non-Photosynthetic Vegetation (NPV)*
Vertical Structure of Fuels	Shade Fraction*
Percent Moisture Content	
Live	Equivalent Liquid Water Thickness**
Dead	na
Species Composition	Classification
Ignition Properties	
Indirect Measures of Above	
Collateral Information (GIS)	
Fire history (Stand age), soils (Site quality), DEM (Insolation, moisture, site quality)	

* From Spectral Mixture Analysis (SMA), Adams et al., (1993); Roberts et al., (1993)
** Green et al., (1993); Roberts et al., (1997a).

3 Methods

3.1 Data

In order to map fuels and monitor seasonal and interannual changes in vegetation, seasonal pairs of AVIRIS data were acquired in the spring and fall of 1994, 1995 and 1997. Due to poor atmospheric conditions during the spring of 1996, no AVIRIS scenes were acquired at that time. However, AVIRIS data were acquired on 17 and 23 October, 1996, before and after the Calabasas fire. In order to cover the entire range, at least two flight lines were flown with each date, one due east and one due west. A minimum of 17 scenes were required to cover the entire range for each date.

Supporting field data for image analysis and accuracy assessment were acquired during several field campaigns in 1995, 1996 and 1997. Field data included spectral reflectance measurements of a homogeneous ground target at Zuma beach during each AVIRIS overpass using an Analytical Spectral Devices (ASD) full range instrument on loan from JPL. Additional spectral data were acquired to develop a regionally specific spectral library for the area (Roberts et al., 1997b) consisting of soils and plant spectra of all chaparral and non-chaparral dominants during the spring and fall (see Gardner, 1997 and Ustin et al., 1998). Additional leaf and branch spectra were collected in the field for later measurement using a Cary-5 laboratory spectrometer at UC Davis. Data for accuracy assessment included close to 300 polygons covering all dominant natural cover types in the region. Data recorded for each polygon included percent cover and species composition. Initial accuracy assessment is summarized in Gardner (1997).

3.2 AVIRIS Processing

Scenes acquired in fall 1994, spring 1995, both dates in 1996 and spring 1997 were processed to retrieve surface reflectance, map column water vapor and equivalent liquid water thickness using the approach of Green et al., (1993). Once processed to apparent reflectance, spectral fractions for green vegetation , non-photosynthetic vegetation, soils and shade were mapped using simple spectral mixture analysis and reference endmembers (Adams et al., 1993; Roberts et al., 1993, 1997c; Ustin et al., 1998). Reference endmembers for the simple models were selected using the approach described by Smith et al. (1990) and Roberts et al., (1997c) from regionally specific spectral libraries developed for the Santa Monica Mountains. During this process, three sets of three endmember models (GV-NPV-shade, GV-Soil-Shade, NPV-Soil-Shade) were generated for each image, then compared to select the model that provided the minimum RMS error and generated physically reasonable fractions for each endmember. A similar approach, based on minimum RMS is described by Painter et al., (1998).

Species maps were generated for each image using Multiple Endmember Spectral Mixture Analysis (MESMA: Roberts et al., 1998), using the modified approach described by Gardner (1997) and Roberts et al., (1997b). MESMA differs from simple spectral mixture models in that it allows the number and types of endmembers to vary on a per-pixel basis. In this manner, it overcomes some of the errors inherent in simple mixture models (e.g., fraction errors, endmember ambiguity), while significantly increasing the number of materials that can be mapped as distinct from their spectra. To date, MESMA has been applied to map snow grain size and snow covered area (Painter et al., 1997), semi-arid vegetation (Okin et al., 1998) and chaparral (Gardner, 1997; Roberts et al., 1997b;1998) and is currently being applied to boreal forest and temperate rain forest. Vegetation maps developed using MESMA are currently limited to fall 1994 and fall 1996 because the spring library is still being organized. All AVIRIS products, including maps of column water vapor, liquid water, spectral fractions and vegetation dominants were coregistered to a georeferenced SPOT Image available from the U.C. Santa Barbara Map and Imagery Library, resampled to a 20 meter resolution.

3.3 GIS Layers

GIS layers developed for the study included a digital elevation model, fire history from 1925 to 1996 and 1930s vegetation (Weislander and Gleason, 1954; Office of Emergency Services, 1995). Fire history maps, developed by the Los Angeles County Fire Department, were processed to develop maps showing the age of the last fire and fire frequency since 1925.

4 Results

A summary of the data developed for this project is shown in Table 2. Fully georeferenced products are available for the entire range (17+ scenes) for fall 1994, spring 1995, fall 1996 (pre and post Calabasas fire) and spring 1997. Spectral fractions have been generated for all of the images described. MESMA-derived vegetation maps have only been generated for fall images. Fuels, destructively harvested by the USDA forest service in 1995, have been located in the GIS. These are currently being used to develop a model that relates AVIRIS fraction images, vegetation cover and liquid water to fuels sampled on the ground. A specific, near-term objective has been to develop fuels layers for the Calabasas area before and after the fire in 1996, and use these data as inputs into a fire-spread model to simulate the Calabasas fire. The fire spread simulation will be conducted by Dr. Jim Bossert, of Los Alamos National Laboratory.

Table 2. AVIRIS products. Products are labeled as none, incomplete (inc) or complete (com). Incomplete means some, but not all scenes have been processed. Complete processing covers the entire range.

Date	Reflectance Retrieval		Spectral Fractions				MESMA	Georeferencing
	Liquid Water	Water Vapor	GV	NPV	Soil	Shade		
940411	Inc	Inc	None	None	None	None	None	None
941019	Com	Com	Com	Com	Com	Com	Com	Com
950509	Com	Com	Com	Com	Com	Com	Com	Com
950526	Inc	Inc	None	None	None	None	None	None
951012	Inc	Inc	None	None	None	None	None	None
951020	Inc	Inc	None	None	None	None	None	None
951026	Inc	Inc	None	None	None	None	None	None
961017	Com	Com	Com	Com	Com	Com	Com	Com
961023	Com	Com	Com	Com	Com	Com	Com	Com
970407	Com	Com	Com	Com	Com	Com	Com	Com

Some of the potential of liquid water and spectral fractions as indicators of fire hazard are illustrated for the Calabasas fire (Figs. 1& 2). Liquid water was mapped for 17 October and 23 October , several days before and after the fire (Fig. 1). The fire began in the north-central portion of the region, in an area dominated by grasslands and coastal sagebrush, mapped as having low liquid water (Fig. 1). It spread rapidly southwards until it reach the vicinity of Malibu Canyon where it slowed significantly, then crossed through rugged terrain and moved rapidly to the coast. Once at the coast it burned west and northwest, burning chaparral to the northwest and coastal sagescrub and grasslands to the west. On the post-fire liquid water image (Fig.1, right frame), the fire scar is clearly indicated by a region of low liquid water due to the removal of most green vegetation. Spectral fractions of the same region (Fig. 2) provide more detailed information regarding surface cover before and after the fire. For example, the region where the fire started (northeast portion of image) was modeled as consisting of high fractions of NPV and low fractions of GV and soil (Fig 2., a to c). Once it progressed to the coast, the fire was restricted primarily to regions mapped as having low GV and higher NPV fractions, a noteworthy exception being the central portion of the area, which consisted of hard chaparral and had higher GV and lower NPV fractions. The post-fire image shows the fire-scar as consisting primarily of soil, which had replaced either GV or NPV depending on the vegetation type.

5 Summary

AVIRIS has the potential of significantly improving our capability to assess fire hazard through improved mapping of vegetation and fuels properties. Critical AVIRIS capabilities include robust retrieval of apparent surface reflectance, the capability of mapping canopy liquid water and improved classification of vegetation. Spectral mixture analysis, applied to reflectance data using reference endmembers adds additional relevant information including estimates of green (live) and non-photosynthetic fuels. In this paper, we describe the data layers we have been developing from AVIRIS which will be used to assess fire hazard and simulate fire spread in the Santa Monica Mountains. Near-term objectives of this project include integrating AVIRIS products with field measures of wildland fuels, then incorporation of spatially explicit maps of fuels in a fire spread model. One key objective will be to test the sensitivity of fire spread simulations to fuels using the pre and post Calabasas AVIRIS data sets.

6 Acknowledgements

Support for this research was provided by grants from the National Aeronautics and Space Administration, Terrestrial Ecosystems and Biogeochemical Dynamics Branch, and Solid Earth and Natural Hazards program (NAGW-4626-I and NAG2-1140). Computer equipment was supplied as part of a start-up package at U.C. Santa Barbara in the Department of Geography and through a UCDRD grant for collaborative research with Los Alamos National Laboratory (STB/UC:97-50). Coregistration software was kindly supplied by J. Steven Cothern of the University of Washington. Field spectral measurements were collected using equipment on loan from the Jet Propulsion Laboratory. A portion of this research was carried out at the Jet Propulsion Laboratory, California Institute of Technology, under a contract with the National Aeronautics and Space Administration.

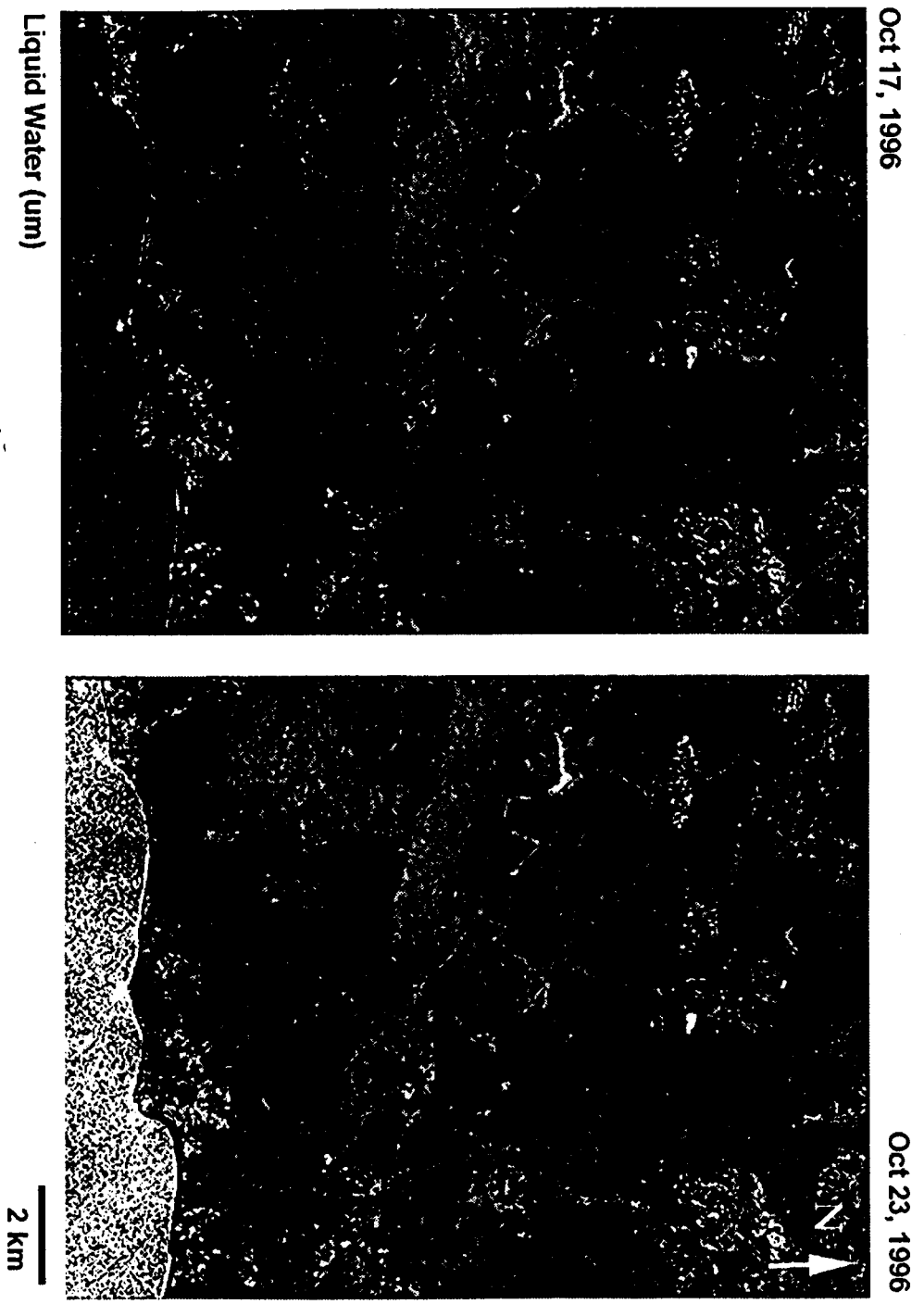

Figure 1. Equivalent liquid water images of the Calabasas area before and after the Calabasas fire.

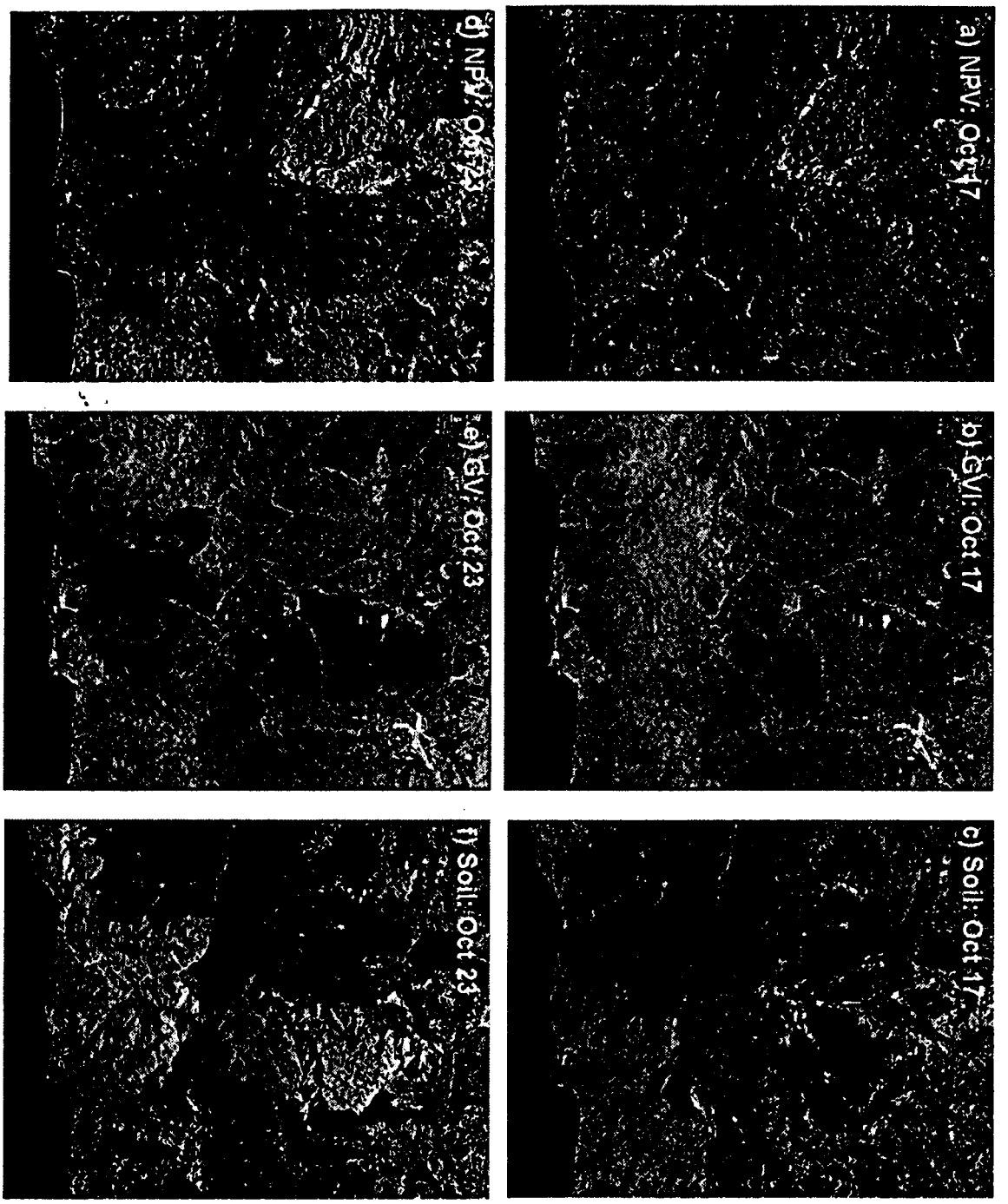

Figure 2. Fraction images for NPV, GV, and Soil for the Calabasas area before and after the fire.

7. References

Adams, JB, Smith, MO and Gillespie, AR, 1993, Imaging spectroscopy: Interpretation based on spectral mixture analysis, In Pieters C.M., and Englert, P., eds. Remote Geochemical Analysis: Elemental and Mineralogical Composition 7: 145-166, Cambridge Univ. Press., NY.

Burgan, RE, and Shasby, MB, 1984, Mapping broad-area fire potential from digital fuel, terrain and weather data, *J. For.*, 8: 228-231.

Clarke, KC, Brass, JA, and Riggan, PJ, 1994. A cellular automaton model of wildfire propagation and extinction. *Photogramm. Eng. Remote Sens* 60(11): 1355-1367.

Chuvieco, E, and Congalton, RG, 1989, Application of remote sensing and geographic information systems to forest fire hazard mapping, *Rem. Sens. Environ*, 29:147-159.

Cohen, WB, 1991, Chaparral vegetation reflectance and its potential utility for assessment of fire hazard, *Photogramm. Eng. Remote Sens* 572: 203-207

Cosentino, MJ, Woodcock, CE, and Franklin, JE, 1981, Scene analysis for wildland fire fuel characteristics in a mediterranean climate., Presented at the 15th Int. Symp. Rem. Sens. Environ., Ann Arbor, MI, 1981, 11 pp.

Gardner, M, 1997, Mapping chaparral with AVIRIS using advanced remote sensing techniques, University of California Masters Thesis, 58 pp.

Gomes, D, Graham, OL, Marshall, EH and Schmidt, AJ, 1993, Sifting through the ashes, lessons learned from the Painted Cave Fire, South Coast Historical Series, Graduate Program in Public Historical Studies, Univ. of California, Santa Barbara, 194 pp.

Green, RO, Conel, JE and Roberts, DA, 1993, Estimation of Aerosol Optical Depth and Additional Atmospheric Parameters for the Calculation of Apparent Surface Reflectance from Radiance Measured by the Airborne Visible-Infrared Imaging Spectrometer (AVIRIS), *Summaries of the 4th Annual JPL Airborne Geoscience Workshop, Oct 25-29,* Vol. 1. AVIRIS Workshop, Washington D.C., 73-76.

Office of Emergency Services (1995), Santa Monica fire history maps, 1935 to 1954, 1954 to 1974 and 1974 to 1994, Joint OES-FEMA Disaster Field Office, 245 S. Los Robles Ave., 4th floor, Pasadena, CA, 91101.

Okin, GS, WJ Okin, DA Roberts, and BC Murray, 1998. Multiple endmember spectral mixture analysis: application to an arid/semi-arid landscape, this volume.

Painter, TH, Roberts, DA, Green, RO, Dozier, J, 1997, Estimating Snow Cover and Grain Size from AVIRIS data with Spectral Mixture Analysis and Modeled Snow Spectra, in SPIE Conf. Vol 3118, Imaging Spectrometry III, 12 p., San Diego, CA July 27-Aug 1, 1997.

Painter, TH, Roberts, DA, Green, RO, and Dozier, J., 1998, Improving Mixture Analysis Estimates of Snow-Covered Area from AVIRIS Data, *Rem. Sens. Environ.* in press.

Philpot, CW, 1977, Vegetative features as determinants of fire frequency and intensity. Presented at the Symposium on Environmental Consequences of Fire and Fuel Management in Meditteranean Ecosystems, Palo Alto, CA, Aug 1-5, 1977, pp. 12-16.

Roberts, DA, Adams, JB, and Smith, MO, 1993, Discriminating Green Vegetation, Non-Photosynthetic Vegetation and Soils in AVIRIS Data, *Rem. Sens. Environ.*, 44: 2/3 255-270.

Roberts, D.A., Gardner, M., Church, R., Ustin, S., Scheer, G.,and Green, R.O., 1998, Mapping Chaparral in the Santa Monica Mountains using Multiple Endmember Spectral Mixture Models, *Rem. Sens. Environ.* in press.

Roberts, DA, Green, RO, and Adams, JB, 1997a,Temporal and Spatial Patterns in Vegetation and Atmospheric Properties from AVIRIS, *Remote Sens. Environ* 62: 223-240.

Roberts, DA, Gardner, M, Church, R, Ustin, SL, and Green, RO, 1997b, Optimum Strategies for Mapping Vegetation using Multiple Endmember Spectral Mixture Models, in SPIE Conf. Vol 3118, Imaging Spectrometry III, 12 p., San Diego, CA July 27-Aug 1, 1997.

Roberts, DA, Batista, G, Pereira, J, Waller, E, and Nelson, B, 1997c, Change Identification using Multitemporal Spectral Mixture Analysis: Applications in Eastern Amazonia, in Remote Sensing Change Detection: Environmental Monitoring Applications and Methods, (Elvidge, C. and Lunetta R., Eds.), Ann Arbor Press, Ann Arbor, MI, in press.

Smith, MO, Ustin, SL, Adams, JB, and Gillespie, AR, 1990, Vegetation in deserts: I A regional measure of abundance from multispectral images, *Remote Sens. Environ.*, 31: 1-26.

Stow, D. Hope, A., McKinsey, D., and Pray, H., 1993, Deriving dynamic information on fire fuel distribution in southern California chaparral from remotely sensed data., *Landscape and Urban Planning*, 24: 113-127.

Ustin, SL, Roberts, DA, Scheer, G., Castaneda, CM, Jacquemoud, S., Pinzon, J., and Palacios, A., 1997, Estimating Canopy Water Content of Chaparral Shrubs Using Optical Methods, *Rem. Sens. Environ.* in press.

Wieslander, AE, and Gleason, CH, (1954), Major brushland areas of the Coastal Ranges and Sierra Cascades Foothills in California, USDA Forest Service, California Forest and Range Experiment Station miscellaneous paper 15.

Yool, SR, Eckhardt, DW, and Cosentino, MJ, 1985, Describing the brushfire hazard in southern California. *Anal. Assoc. Am. Geograph.* 75: 431-442.

INVESTIGATING THE RELATIONSHIP BETWEEN LIQUID WATER AND LEAF AREA IN CLONAL POPULUS

Dar Roberts[1], K. Brown[2], R. Green[13], S. Ustin[4] and T. Hinckley[2]

1. Department of Geography, EH3611, University of California, Santa Barbara, CA 93106
2. College of Forestry, University of Washington, Seattle, WA 98195
3. Jet Propulsion Laboratory, California Institute of Technology, 4800 Oak Grove Dr., Pasadena, CA 91109
4. Department. of Land, Air, and Water Resources, University of California, Davis, CA, 95616,

1 Introduction

Leaf Area Index (LAI) is one of the most commonly employed biophysical parameters used to characterize vegetation canopies and scale leaf physiological processes to larger scales. For example, LAI is a critical parameter used in regional scale estimates of evapotranspiration, photosynthesis, primary productivity, and carbon cycling (Running et al., 1989; Dorman and Sellers, 1989; Potter et al., 1993). LAI is typically estimated using ratio-based techniques, such as the Normalized Difference Vegetation Index (NDVI: e.g. Tucker 1979; Asrar et al. 1989; Sellers 1985; 1987). The physical basis behind this relationship depends on the high spectral contrast between scattered near-infrared (NIR) and absorbed red radiation in canopies. As the number of leaves present in a canopy increases over a unit area, NIR reflectance increases, while red reflectance decreases, resulting in an increase in the ratio. Through time series and image compositing, NDVI provides an additional temporal measure of how these parameters change, providing a means to monitor fluxes and productivity (Tucker et al., 1983). NDVI, while highly successful for agriculture and grassland ecosystems has been found to be less successful in evergreen chaparral and forested ecosystems (Badhwar et al., 1986; Gamon et al., 1993; Hall et al., 1995). Typically, the relationship between NDVI and LAI becomes progressively more asymptotic at LAI values above three (Sellers, 1985), although linear relationships have been observed in conifers at LAIs as high as 13 for some conifers (Spanner et al., 1990).

In this paper, we explore an alternative approach for estimating LAI for remotely sensed data from AVIRIS based on estimates of canopy liquid water. Our primary objective is to test the hypothesis that the depth of the liquid water bands expressed in canopy reflectance spectra at 960, 1200, 1400 and 1900 nm increases with increasing LAI in canopies. This study builds off of work by Roberts et al. (1997), in which liquid water was shown to increase following a gradient of increasing LAI ranging from grasslands to coniferous forests. In that study, it was observed that forests, which showed little variation in NDVI, showed significant variation in liquid water. In order to test this hypothesis, we analyzed field spectra measured over *Populus* shrubs of known LAI and monitored changes in liquid water in young *Populus* stands as they aged over a four year time span. The study was conducted in south-central Washington, in a clonal *Populus* fiber farm owned and operated by Boise-Cascade near the town of Wallula.

2 Background

2.1 Estimation of Liquid Water in Canopies

Green et al., (1991,1993) developed techniques for retrieving apparent surface reflectance, mapping column water vapor and liquid water from AVIRIS using a modified version of Modtran radiative transfer code. In order to separate water vapor in the atmosphere from liquid water in the landscape, Green et al., (1993) incorporated a simple model for the expression of liquid water in a reflectance spectrum. This model makes the assumption that the depth of the liquid water band across the 865 to 1035 nm region can be approximated using Beer-Lamberts law for exponential extinction in an absorbing or scattering medium. Based on this model, the depth of the water band will vary as a function of the strength of the absorber (described by the absorption coefficient for liquid water) and the pathlength of light within an absorbing/ scattering element. While this simple model was originally developed primarily to improve water vapor retrievals from AVIRIS, recent studies by Roberts et al., (1997) and Ustin et al. (1998) have shown that the liquid water maps that result may be one of the most products available from AVIRIS.

In order to simulate AVIRIS liquid water retrievals in field spectra, a Beer-lambert model was developed that duplicates the approach used in AVIRIS. This approach is shown schematically in Figure 1. In the upper two frames, two formulations of the Beer-Lambert law are presented, one that models light attenuated as it passes through an absorbing (or scattering) medium, and one in which part of the light is partially blocked. In the example shown on the left, the natural log of transmittance (or reflectance) can be modeled as linear function that passes through the origin and has a slope equal to the pathlength. Addition of a blocking factor adds an intercept to the equation. In the central frames, two leaf reflectance spectra are shown on the left, with a plot of the absorption coefficient of liquid water on the right. The lowest frame shows a plot of ln(R) against the absorption coefficient for two wavelength regions. Liquid water thickness would be reported as the slope of the line.

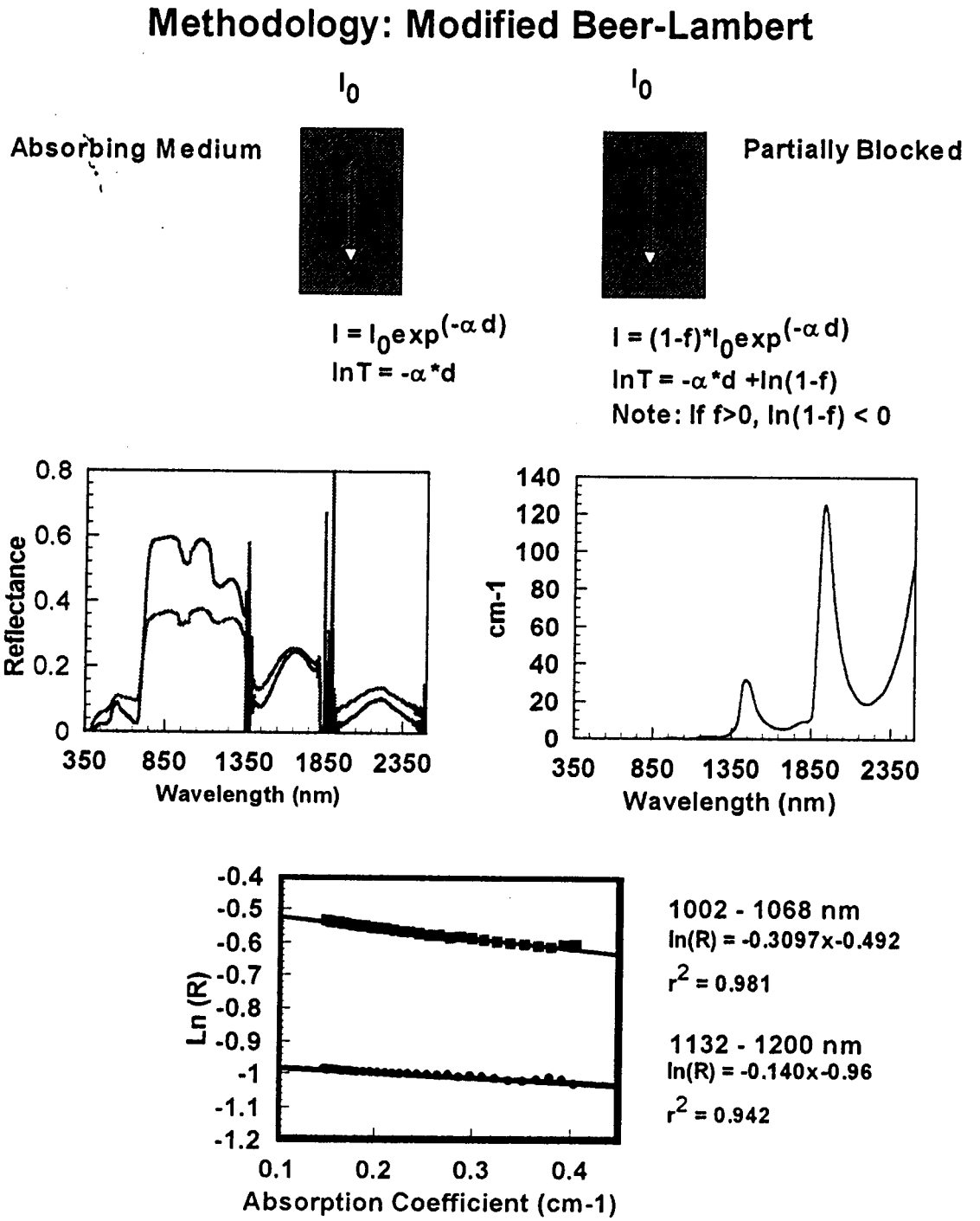

3 Methods

3.1 Study Site

The study was conducted in the vicinity of Wallula, Washington (46° 4' N, 118° 54' W), located several km southeast of the confluence of the Snake and Columbia Rivers. The area has a semi-arid, steppe climate, characterized by minimum monthly temperatures slightly below freezing between the months of December and February and peak summer temperatures above 30° C in July and August (Environmental Data Service, 1994;1996). Total annual precipitation ranges between 200 and 350 mm, falling primarily between November and February, but extending through all months except July and August. The dominant natural vegetation is sagebrush scrub (*Artemisia tridentata*), although the region has extensive agricultural development growing potatoes, corn, and other agricultural crops. Field research and image analysis concentrated at the Boise-Cascade Wallula fiber farm, a plantation consisting primarily of *Populus trichocarpa, nigra* and *deltoides* clones (Fig. 2). *Populus* clones in the area begin to leaf out in April, reach peak leaf display by June then senesce by October, varying slightly each year depending on annual temperature. Spectral differences between *trichocarpa-deltoides* (TxD) and *deltoides-nigra* (DXN) can be attributed primarily to architectural differences between TxD with more horizontally oriented leaves and DxN with more vertical leaf displays (Roberts et al., 1995; Hielman et al., 1996).

3.2 Field Study

The field study was designed to test the LAI/liquid water hypothesis using field spectra of DxN clones at the Wallula fiber farm. Field work was conducted at the farm between July 20th and July 25th, 1997 during the time of an AVIRIS overflight. Seventy six young stump sprouting plants, ranging between 10 and 60 cm in height were located and flagged in a 6 year old stand that had been recently harvested. Reflectance spectra were measured of each plant using an Analytical Spectral Devices (ASD) full range instrument on loan from JPL (Analytical Spectral Devices, Boulder, CO). Field spectra were standardized to spectralon (Labsphere, Inc. North Sutton, NH) measured at approximately 10 minute intervals. At least three replicates were measured for each plant. One to four sets of spectra were measured at each plant depending on the size of the shrub at a height of 0.5 m above the canopies.

For destructive harvesting the plants were stratified into five height classes: < 19 cm, 20-29 cm, 30-37 cm, 38-48 cm and 48-60 cm. Five plants were randomly sampled from each height class for detailed analysis. Measurements of plant height, and diameter along the major and minor axes were collected for each of the sampled plants for later determination of ground area and plant volume. In order to determine leaf area of each of the sample plants, every stem was destructively harvested then measured with calipers to determine stem diameter. In order to develop a linear equation that relates leaf area to stem diameter, one of every ten stems was stored in a plastic bag and cooled for later laboratory analysis. In the laboratory, leaves from each stem were harvested, measured for leaf area then regressed against stem diameter. Once this relationship had been developed, it was combined with the shrub stem data to calculate total leaf area for each shrub, then divided by the areal projection of each shrub (in meters) to determine LAI. An example for plant 6-7 (row 6, 7th plant), which consisted of 353 stems is shown in Figure 3.

Liquid water was determined from leaf spectra using the approach described in the background section, modified to account for differences between AVIRIS spectra and the field spectra. The most notable difference occurs in the transition between the VNIR and SWIR1 detectors in the instrument used in the field. Instrumental problems between the VNIR (350-1000 nm) and SWIR1 (1000-1800 nm) regions, tend to create a discontinuity between the two detectors in reflectance spectra (Fig. 1). As a result, it was not possible to apply the same wavelength range as used in AVIRIS to the field spectra. As a solution, the liquid water fits were restricted to the long-wavelength end of the liquid water band, ranging from 1002-1068 nm rather than the 865 to 1065 nm region used in AVIRIS. To test whether AVIRIS and ASD data gave similar results in a wavelength region that did not have instrumental artifacts, fits were also extended to the 1132-1200nm and applied to both field and AVIRIS reflectance spectra.

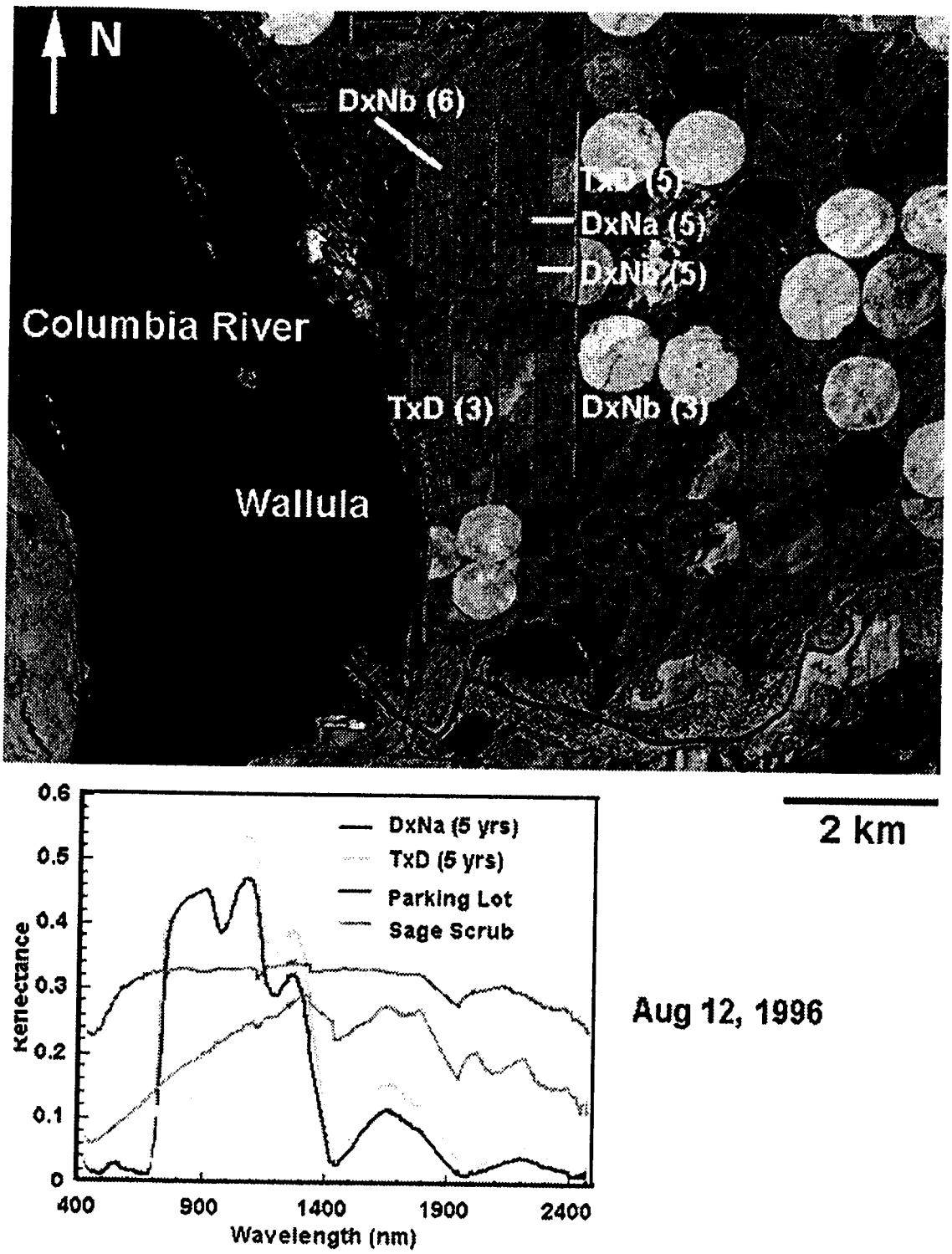

Figure 2. Index map of Wallula fiber farm. Reflectance spectra are displayed for DXN, TXD clones, sage scrub and a parking lot, which was used as a temporally invariant target for calibration.

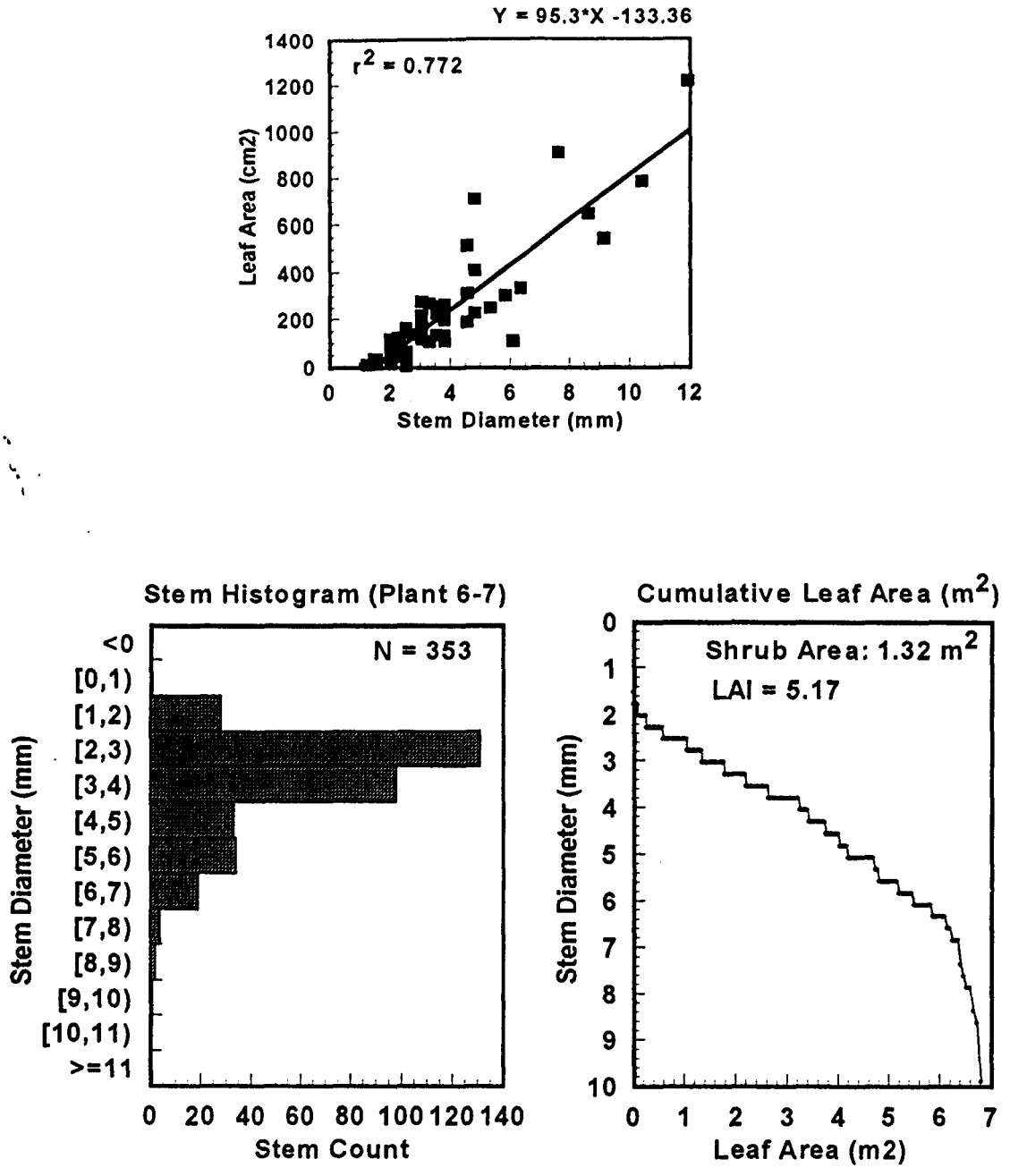

Figure 3. Stem diameter, leaf area relationship. An example calculation is shown for Plant 6-7.

3.3 AVIRIS Processing

An alternate approach, based off of multitemporal AVIRIS data was used to determine whether changes in canopy liquid water matched expected patterns in leaf area development as stands aged. In order to test this hypothesis, five AVIRIS scenes were analyzed over the study site, acquired primarily within a seasonal window after full leaf area development in early June and prior to senescence in October. Data sets acquired during this window included September 22, 1994, June 12 and August 18, 1996 and July 23 1997. A late season data set, acquired on October 18, 1995, showed early signs of senescence in most of the clones.

Once acquired, reflectance was retrieved and liquid water and water vapor mapped for each scene using the modified Modtran-2 radiative-transfer approach described by Green et al., (1993) and Roberts et al. (1997). Field spectral data from two bare soil transects measured in 1997 were used to correct for radiometric and wavelength discrepancies between AVIRIS and modtran. After correcting the 1997 data, a

temporally invariant target was located in the scene and used to improve reflectance retrieval for the remaining scenes from 1994, 1995 and 1996. Example spectra for Aug 12, 1996 are shown in Figure 2.

4 Results

4.1 Field Study

LAI for the 25 study plants ranged between 1.8 for one of the smallest shrubs to 8.75 for one of the largest, with most of the shrubs ranging between 4 and 6.5 (Fig. 4). Liquid water fits ranged between 0.05 and 0.38 cm in the 1002-1068 nm region and 0.025 and 0.23 cm in the 1132-1200 nm region. Lower liquid water estimates at the longer wavelength are consistent with the fact that the 1132-1200 nm water band is a stronger absorption feature and thus scattered NIR light will penetrate to a shallower depth within the crown. When plotted against liquid water, estimated from the spectral data, LAI and liquid water proved to have a positive, linear relationship with r^2 values of 0.646 and 0.721 in the 1002-1068 and 1132-1200 nm liquid water absorptions (Fig. 4). Differences in the slopes of these linear relationships can also be attributed to the greater strength of the 1132-1200 nm water band.

The validity of the LAI-liquid water relationship is supported by analysis using more standard approaches such as the NDVI (NIR-red)/(NIR+red) and VI (NIR/red). For example, the plot of NDVI against LAI demonstrates that the NDVI becomes progressively more asymptotic with increasing LAI, matching most published observations. The VI, in contrast, shows a much more linear relationship, showing only slightly lower fits than liquid water. In both cases, liquid water provides the superior estimate and shows a linear relationship even to the highest value observed in the shrubs.

4.2 AVIRIS Multitemporal Study

Based on prior work with the clonal *Populus*, leaf area would be expected to reach peak development in June, sustain a high level throughout the summer, then begin to senesce in the Fall, during October. As a result, with the exception of the 1995 data, differences in LAI observed from 1994 to 1997 should be a product of long term differences in stand age, not phenological changes. Between 1994 and 1997, stand age varied between less than one year to over six years. Over this period of time, LAI would be expected to show yearly increases for the first three years, followed by slight declines over the remaining three years (Heilman et al., 1996).

In order to test whether the expected patterns were observed in liquid water, four stands (plus replicates) were located in the study site, two stands that were originally planted in 1992 and two planted during April, 1994. In order to determine whether leaf angles had an impact on the liquid water retrievals, stands were selected both from the clone with more horizontally oriented leaves, TXD and the more vertically oriented DxN. Temporal patterns in liquid water were also compared to the NDVI, to determine whether similar patterns were observed in that measure.

Temporal analysis of the older stands (Fig. 5, top left) demonstrated few changes in liquid water from 1994 to 1997. The only major temporal change was observed in 1995, in which the TxD showed a marked decrease in liquid water and the DxN a slightly lower decrease, attributed to late season senescence and a loss of leaf area. In all cases, the TxD showed a slightly lower liquid water than the DXN, which can be attributed to either lower leaf area, or the effect of differences in leaf angles. In comparison, the NDVI showed little temporal variation (Fig. 5, row 2). Calculation of liquid water directly from AVIRIS reflectance, using the same program used for the field data, yielded similar results to those produced from the reflectance retrieval. Comparison of field data to AVIRIS spectra, demonstrated higher liquid water estimates for full stands relative to small shrubs, equal to close to 1 mm of water.

Analysis of changes in liquid water in the younger stands demonstrated a uniform increase in liquid water over the first three years, followed by a slight decline in the fourth year (Fig. 5, top right). Unlike observations in the older stands, NDVI showed marked changes, dramatically increasing in the first two years followed by little change in the third year. The VI was not calculated because it proved too sensitive to minor atmospheric correction problems in the red wavelengths.

Patterns in the liquid water matched expected patterns based on stand age and seasonality. In comparison, the NDVI shows little variation except in very young stands.

LAI Compared to Liquid Water

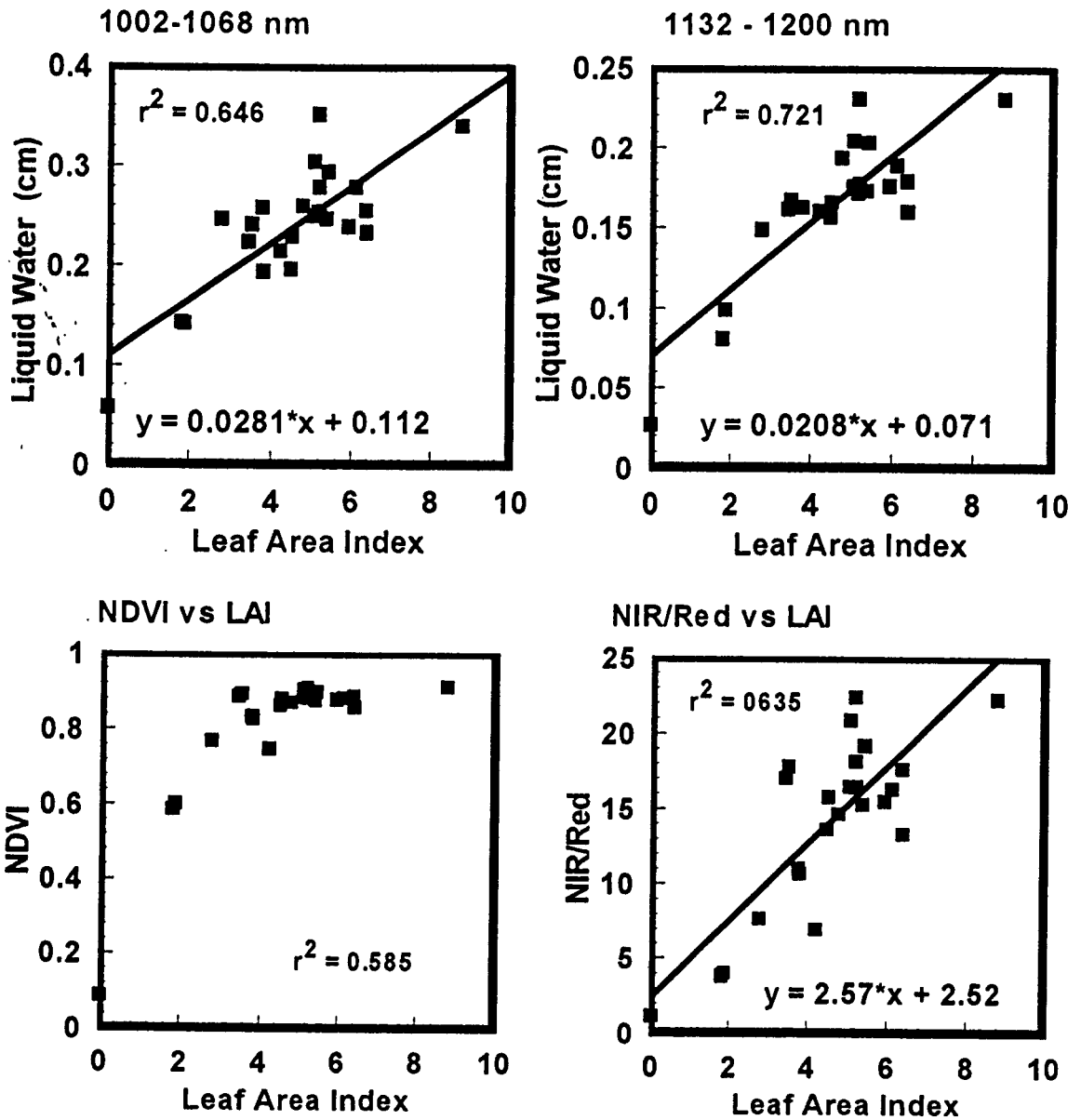

Figure 4. Comparison of LAI to liquid water thickness, NDVI and VI.

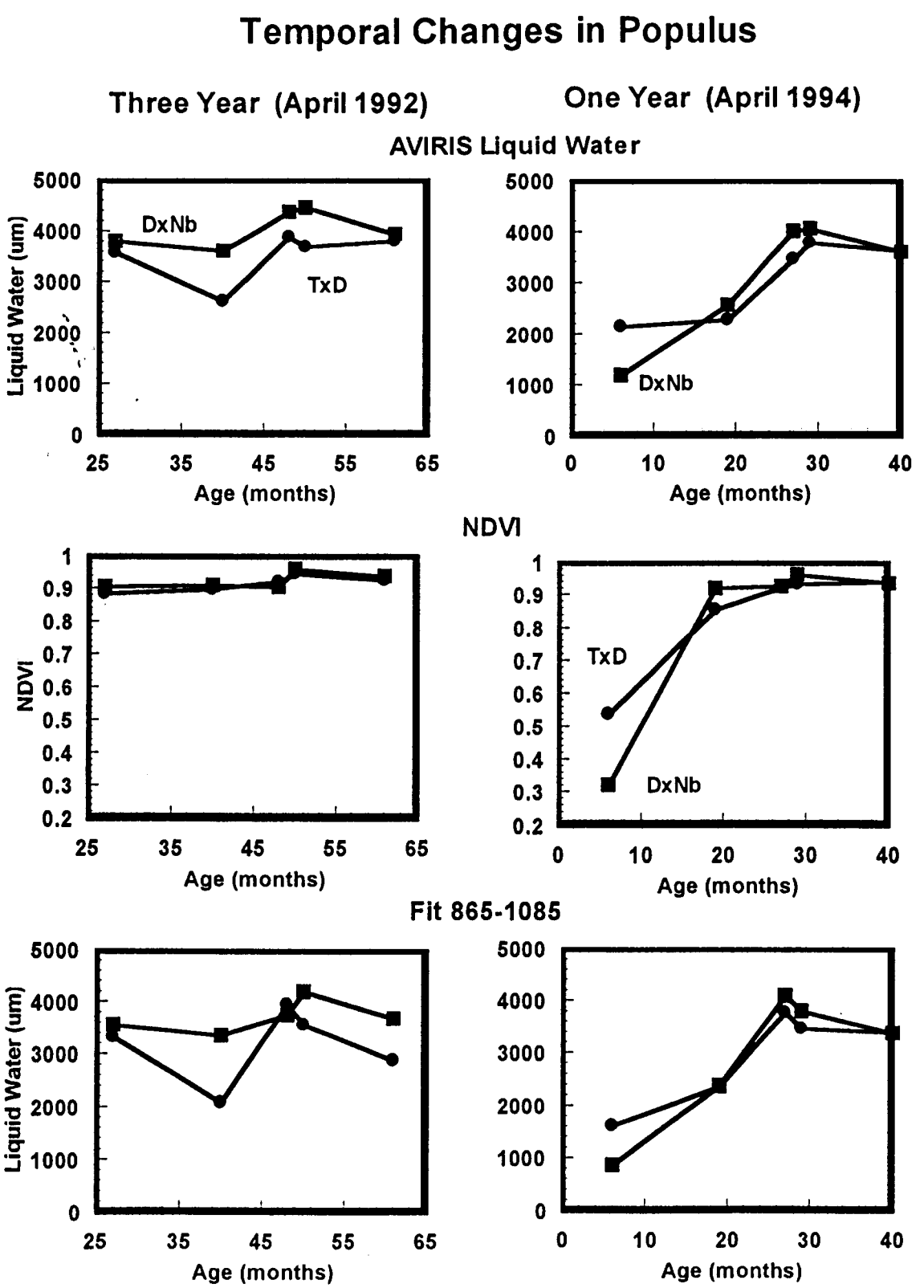

Figure 5. Temporal changes in liquid water and NDVI for select Populus stands from 1994 to 1997. Plots to the left show results for stands planted in 1992, plots on the right show stands planted in 1994.

5. 0 Summary

In this study we tested the hypothesis that LAI is linearly related to liquid water. There were two components of the study, a field study using reflectance measurements of *Populus* shrubs which were harvested to determine LAI and a temporal study of AVIRIS data that tracked changes in liquid water as stands aged over a four year period. The field study demonstrated that LAI and liquid water are linearly correlated up to LAI 8.75. In comparison, the NDVI/LAI relationship showed the expected asymptotic relationship which saturated near an LAI of 3.0. The VI showed a surprisingly good linear relationship.

AVIRIS analysis showed temporal patterns in the liquid water which matched expected patterns based on stand age and seasonality. In this instances, the only significant pattern in the older stands was due to senescence in the October, 1995 data set. In the younger stands, liquid water increased for the first three years followed by a decline in the fourth year. In comparsion, the NDVI showed little variation except in very young stands.

These results suggest that liquid water retrieved from AVIRIS may form a new, potentially powerful technique for mapping stand structure. However, there remain several important research directions that should be pursued. These include sensitivity analysis to determine how relationship varies between very different types of vegetation (e.g. shrubs, conifers) and how it varies seasonally with water status (as in chaparral). Furthermore, methods should be explored that avoid the use of correlative relationships between field data and remotely sensed measures of liquid water.

6 Acknowledgements

Support for this research was provided by DOE grant W/GEC95-062A as part of the Westgec program. AVIRIS data used in this study were acquired by NASA. Computer equipment was supplied as part of a start-up package at U.C. Santa Barbara in the Department of Geography and through a UCDRD grant for collaborative research with Los Alamos National Laboratory (STB/UC:97-50). Field spectral measurements were collected using equipment on loan from the Jet Propulsion Laboratory. A portion of this research was carried out at the Jet Propulsion Laboratory, California Institute of Technology, under a contract with the National Aeronautics and Space Administration. In particular, we wish to thank Boise-Cascade for allowing access to the Wallula fiber farm and their readiness to supply supporting information and technical assistance since 1994.

7 References

Adams, JB, Smith, MO and Gillespie, AR, 1993, Imaging spectroscopy: Interpretation based on spectral mixture analysis, In Pieters C.M., and Englert, P., eds. Remote Geochemical Analysis: Elemental and Mineralogical Composition 7: 145-166, Cambridge Univ. Press., NY.

Asrar, G, Myneni, RB, and Kanemasu, ET, 1989, Estimation of plant-canopy attributes from spectral reflectance measurements, in Theory and Applications of Optical Remote Sensing, (Asrar, G., ed), John Wiley and Sons, NY, 252-296.

Badhwar, GD, MacDonald, RB, and Mehta, NC, 1986,.Satellite-derived leaf-area-index and vegetation maps as input to global carbon cycle models - a hierarchical approach, 7(2): 265-281. *Int. J. Remote Sens.*

Dorman, JL, and Sellers, PJ,1989.A Global Climatology Albedo, Roughness Length and Stomatal Resistance for Atmospheric General Circulation Models as Represented by the Simple Biosphere Model (SiB). *J. Applied Met.* 28:833-855

Gamon, J. A., Field, C.B., Roberts, D.A., Ustin, S.L., and Riccardo, V.,1993, Functional Patterns in an Annual Grassland during an AVIRIS Overflight, *Rem. Sens. Environ.*, 44: 2/3: 239-253.

Green, RO, Conel, JE, Margolis, JS, Bruegge, CJ, and Hoover, GL,1991, An inversion algorithm for retrieval of atmospheric and leaf water absorption from AVIRIS radiance with compensation for atmospheric scattering, in *Proc. 3rd Airborne Visible/Infrared Imaging Spectrometer (AVIRIS) Workshop* (R.O. Green Ed.), Pasadena, CA 20-21 May, pp. 51-61.

Green, RO, Conel, JE and Roberts, DA, 1993, Estimation of Aerosol Optical Depth and Additional Atmospheric Parameters for the Calculation of Apparent Surface Reflectance from Radiance Measured

by the Airborne Visible-Infrared Imaging Spectrometer (AVIRIS), *Summaries of the 4th Annual JPL Airborne Geoscience Workshop, Oct 25-29,* Vol. 1. AVIRIS Workshop, Washington D.C., 73-76.

Hall, FG, Shimabukuro, Y, and Huemmrich, KF, (1995), Remote sensing of forest biophysical structure using mixture decomposition and geometric reflectance models, *Ecological Applications*, 5(4): 993-1013.

Heilman, PE, Hinckley, TM, Roberts, DA, and Ceulemans, R, 1996, Production Physiology, Ch. 18, in Biology of Populus and its Implications for Management and Conservation (Stettler, R., Bradshaw, H., Heilman P., and Hinckley T., Eds)., NRC Research Press, Ottawa.

NOAA National Environmental Satellite, Data and Information Service, (1994), Climatological Data: Washington: 98(1-12):

NOAA National Environmental Satellite, Data and Information Service, (1996), Climatological Data: Washington: 100(1-12):

Potter, CS, Randerson, JT, Field, CB, Matson, PA, Vitousek, PM, Mooney, HA, and Klooster, SA,1993, Terrestrial ecosystem production: a process model based on global satellite and surface data, *Global Biogeochem. Cycles*, 7:811-841.

Roberts, DA, Brown, KJ, Hinckley, TM, Green, RO, and Ustin, SL, 1995, Remote Estimates of Canopy Coupling and Architecture Using an Imaging Spectrometer: Conifer vs. Hardwood, 1995 Ecological Society of America, Snow Bird, Utah, July 30-Aug 3, 1995.

Roberts, DA, Green, RO, and Adams, JB, 1997,Temporal and Spatial Patterns in Vegetation and Atmospheric Properties from AVIRIS, *Remote Sens. Environ* 62: 223-240.

Running, SW, Nemani, R, Peterson, DL, Band, LE, Potts, DF, Pierce, LL, and Spanner, MA, 1989.Mapping regional forest evapotranspiration and photosynthesis by coupling satellite data with ecosystem simulation. *Ecology* 70(4):1090-1101

Sellers, PJ 1985, Canopy reflectance, photosynthesis and transpiration. *Int J. Remote Sens.* 6(8): 1335-1372.

Sellers, PJ,1987,Canopy Reflectance, Photosynthesis and Transpiration. II. The Role of Biophysics in the Linearity of Their Interdependence. *Remote Sens. Environ.* 21: 143-183

Spanner, MA, Pierce, LL, Running, SW, and Peterson, DL ,1990, The seasonality of AVHRR data of temperate coniferous forests: relationship with leaf area index, *Remote Sens. Environ.* 33:97-112.

Tucker, CJ, 1979, Red and photographic infrared linear combinations for monitoring vegetation, *Remote Sens. Environ.* 8:127-150.

Tucker, CJ, Vanpraet, C, Boerwinkel, E, and Gaston, A, 1983, Satellite remote sensing of total dry matter production in the Senegalese Sahel., *Remote Sens. Environ.* 13:461-474

Ustin, S.L., Roberts, D.A., Scheer, G., Castaneda, C.M., Jacquemoud, S., Pinzon, J., and Palacios, A., 1998, Estimating Canopy Water Content of Chaparral Shrubs Using Optical Methods, *Remote. Sens. Environ.* in press.